Mechanical Systems and Signal Processing 162 (2022) 107981

Contents lists available at ScienceDirect

Mechanical Systems and Signal Processing

journal homepage: www.elsevier.com/locate/ymssp

Unstable tilting motion of flexibly supported gas bearing bushings

Philipp Bättig [a], Jürg Schiffmann [a,*]

[a] Ecole Polytechnique Fédérale de Lausanne, EPFL STI IGM LAMD, Maladière 71b, CH-2002 Neuchâtel, Switzerland

ARTICLE INFO

Keywords:
Gas lubricated bearings
Flexible bushing support
Bushing tilting instability
Stabilizing mechanisms

ABSTRACT

This paper presents measurements of the motion amplitudes from flexibly supported Herringbone Grooved Journal Bearing bushings. Measurements taken in four locations on the flexibly supported bearing bushing enable the distinction between the radial and the tilting motion, which allowed to identify an unstable bearing bushing tilting mode. The bushing tilting motion instability can be attributed to the cross-coupled tilting impedance of the gas bearing and its occurrence is characterized by the appearance of a sub-synchronous vibration at the speed of instability onset. The comparison between experimentally obtained data and the prediction of a two degrees of freedom dynamic model that includes the flexible support characteristics, the bushing transverse inertia as well as the gas bearing tilting impedance suggests an excellent agreement on both the Eigenfrequency and the rotor speed of instability onset. Furthermore, the effect of the flexible support tilting stiffness and bearing bushing transverse moment of inertia on the critical bushing tilting speed and onset of tilting instability has been investigated, which led to a design guideline to avoid the onset of an unstable bush tilting mode. In addition, experimental data gathered after the introduction of damping in the flexible support of the bearing bushing suggests a significant increase of the onset speed of the unstable bearing bushing tilting mode.

1. Introduction

Herringbone-grooved Journal Bearings (HGJBs) offer competitive advantages compared to other bearing technologies, such as oil-free operation, low specific losses and the potential to achieve very high rotor speeds. However, in order to ensure stable rotor operation they require very small clearance to diameter ratios h_r/D_{Brg} [1]. For HGJB supported rotors featuring large bearing distance to diameter ratios ($l/D_{Brg} \geqslant 5$), the manufacturing of rigidly supported bushings is challenging and expensive due to the tight bearing clearances and the resulting alignment requirements. Hence, a solution with flexibly supported bushings can offer competitive advantages to mitigate the tight alignment tolerances. Fig. 1 presents such a solution of a bearing bushing supported by means of a flexible membrane, where the radial and the tilting stiffness can be tuned on a wide range by the design of the arms connecting the outer and the inner ring [2]. The flexible support of each bearing bushing is characterized by a radial stiffness k_r and a tilting stiffness k_t, as shown in Fig. 2. Various researchers have investigated ways to increase the stability threshold of HGJBs to allow for a relaxation in the stringent manufacturing tolerances in view of decreasing the manufacturing cost. Most solutions that successfully increase the stability threshold of the rotor-bearing system work on the principle of introducing external damping. This can be achieved by flexibly supporting the bearing bushings on elastomeric O-Rings [3–8], or by using flexible structures that provide Coulomb friction [9,10]. Both methods have shown promising results to increase the stability threshold of HGJBs. Thus, supporting the bearing bushings in a

* Corresponding author.
E-mail address: jurg.schiffmann@epfl.ch (J. Schiffmann).

https://doi.org/10.1016/j.ymssp.2021.107981
Received 21 December 2020; Received in revised form 18 March 2021; Accepted 18 April 2021
Available online 10 May 2021

Nomenclature

Acronyms

HGJB	Herringbone grooved journal bearings
NGT	Narrow groove theory
SIO	Speed of instability onset

Greek Symbols

α	Groove width ratio [–]
β	Groove angle [rad]
Γ	Logarithmic decrement [–]
γ	Whirl speed ratio [–]
ω	Angular frequency, [rad s^{-1}]
Ω_{crit}	Whirl speed ratio of instability onset, [–]
ω_{crit}	Critical angular frequency of bush tilting mode, [rad s^{-1}]
ϕ	Tilting coordinate of bushing [rad]
θ	Tilting coordinate of bushing [rad]

Roman Symbols

$\overline{P}$	Normalized pressure, [–]
A	Vibration amplitude, [m]
C	Radial bearing clearance, [m]
c	Viscous damping coefficient, [N s m^{-1}]
c_t	Tilting damping coefficient, [N s m^{-1}]
C_{ii}	Bearing tilting damping, [N s m^{-1}]
D	Diameter, [m]
D_{Brg}	Bearing diameter, [m]
f	Excitation frequency, [Hz]
h_r	Bearing clearance, [m]
h_r	Groove depth, [m]
J_P	Polar rotor inertia, [kg m^{-2}]
J_{T_B}	Transverse bushing inertia, [kg m^{-2}]
J_{T_R}	Transverse rotor inertia, [kg m^{-2}]
k_r	Radial stiffness, [N m^{-1}]
k_t	Tilting stiffness, [N m rad^{-1}]
K_{ii}	Bearing tilting stiffness, [N m rad^{-1}]
l	Bearing distance, [m]
L_{Brg}	Bearing length, [m]
m_B	Bushing mass, [kg]
m_R	Rotor mass, [kg]
N_{Rot}	Rotor speed, [min^{-1}]
p	Pressure, [Pa]
p_a	Ambient pressure, [Pa]
R	Bearing radius, [m]
T_{ms}	Master slave transformation matrix, [–]
Z_{ii}	Bearing tilting impedance, [N m^{-1}]

flexible manner and applying an optimal combination of support stiffness and damping is suggested to offer a large potential to increase the stability of the rotor-bearing system, while decreasing the manufacturing cost.

1.1. Nature of the issue

The introduction of a flexible support for each individual bearing bushing increases the degrees of freedom of the rotor-bearing system and can potentially induce an unstable motion of the bearing bushings itself. An unstable motion of the bearing bushings can potentially yield very large motion amplitudes, which could cause serious damage. The motion of the bearing bushing can be a pure translational motion, a pure tilting motion or a combination. Radial motion instability has been addressed in prior work [6], however, instability of a bearing bushing in tilting mode has not been reported and addressed yet in the literature.

1.2. Goals and objectives

The objectives of this work are (1) to establish a reduced-order model that allows to capture the tilting motion of flexibly supported gas bearing bushings, (2) to experimentally analyze the motion of a flexibly supported HGJB bushing, (3) to investigate the variables governing the bearing bushing tilting motion and onset of bush tilting instability, (4) to assess the effect of support damping on the onset speed of the bushing tilting instability and (5) to devise design guidelines to avoid the onset of an unstable bearing bushing tilting mode in the nominal speed-range.

1.3. Scope of the paper

In a first step, a reduced-order model is presented to capture the tilting motion of flexibly supported bushings for gas lubricated bearings. In a second step, the experimental setup and the data processing is presented to experimentally investigate the tilting motion of the flexibly supported bearing bushings. In a third step, the effects of tilting stiffness, transverse bushing inertia and support damping on the critical speed of the bush tilting mode and on the onset speed of instability are investigated experimentally and compared to the numerical models. In a last part, the experimental and numerical data are condensed into a simple yet effective design guideline, which offers support to avoid the onset of an unstable bearing bushing tilting mode in the nominal speed range.

2. Methodology

2.1. Dynamic model for the bushing tilting motion

As indicated by the equation of motion for the two bushing tilting axes (see Fig. 6, Eq. (1) and (2)) the tilting motion of a flexibly supported gas bearing bushing is governed by the transverse inertia of the bushing J_{T_B}, the bushing support characteristics (k_t and c_t) and the bearing tilting impedance (K_{ij} and C_{ij}). An underlying assumption leading to Eq. (1) and (2) is that the translational degrees of freedom of the bushing and of the gas bearing supported rotor do not influence the bushing tilting motion.

$$J_{T_B}\ddot{\phi}_B + K_{\phi\phi}\phi_B + K_{\phi\theta}\theta_B + C_{\phi\phi}\dot{\phi}_B + C_{\phi\theta}\dot{\theta}_B + k_t\phi_B + c_t\dot{\phi}_B = 0 \tag{1}$$

$$J_{T_B}\ddot{\theta}_B + K_{\theta\theta}\theta_B + K_{\theta\phi}\phi_B + C_{\theta\theta}\dot{\theta}_B + C_{\theta\phi}\dot{\phi}_B + k_t\theta_B + c_t\dot{\theta}_B = 0 \tag{2}$$

where ϕ and θ are the two tilting degrees of freedom of the bushings. The equations of motion can be rewritten as a matrix system:

$$\mathbf{M}\ddot{\vec{\mathbf{q}}} + \mathbf{C}\dot{\vec{\mathbf{q}}} + \mathbf{K}\vec{\mathbf{q}} = 0 \tag{3}$$

with:

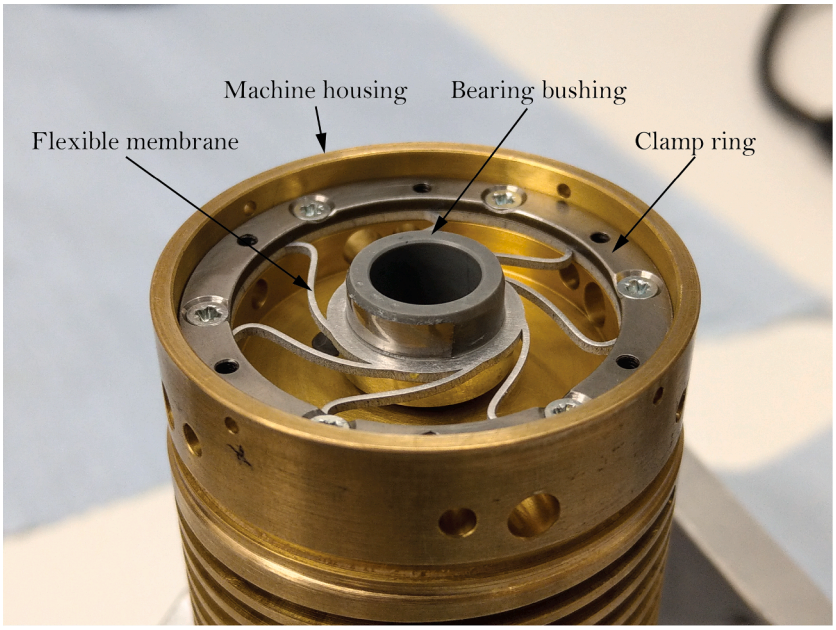

Fig. 1. Bearing bushing supported on flexible membrane and fitted to electric stator.

$$\overrightarrow{\mathbf{q}} = [\phi, \theta]^T \tag{4}$$

The assumption of an appropriate vibrational form such as $\overrightarrow{\mathbf{v}} = \overrightarrow{\mathbf{q}} e^{\delta t}$ transforms Eq. (3) into an Eigenvalue problem with the corresponding Eigenvalues given as follows:

$$\delta_j = \lambda_j + i\gamma_j \Omega_{Rot} \tag{5}$$

where the real part λ_j corresponds to the damping coefficient and the imaginary part $\gamma_j \Omega_{Rot}$ to the damped natural frequency with the whirl speed ratio γ_j. In rotordynamic systems the stability if often quantified using the logarithmic decrement defined as follows:

$$\Gamma_j = -\lambda_j \frac{2\pi}{\gamma_j \Omega_{Rot}} \tag{6}$$

A stable mode requires the logarithmic decrement Γ_j to be positive. Since gas lubricated bearing impedances not only depend on the rotor speed but also on the excitation frequency, the whirl speed map of the bushing tilting motion is obtained by applying Pan's spectral analysis approach [11]. This method consists in exciting the dynamic system over a frequency range ($\omega_{Ex} = \gamma \Omega_{Rot}$ with $\gamma \in [0, 2]$), while keeping the rotor speed Ω_{Rot} fixed. Natural system frequencies and the corresponding damping are identified for a give rotor speed, if both the computed whirl frequency and the excitation frequency coincide.

As suggested by Eq. (1) and (2) the calculation of the tilting Eigenfrequency and damping requires knowledge on the gas bearing impedance in tilting motion. A particular challenge in modeling the static and dynamic behavior of HGJB comes from the presence of the rotating pumping grooves, which yield an unstationary pressure within the fluid film therefore leading to a varying bearing impedance. An elegant way to model HGJB has been introduced by Vohr and Chow [12], who assume an infinite number of grooves. The so called Narrow Groove Theory (NGT), which has been validated experimentally by Guenat and Schiffmann recently [13], leads to a smooth fluid film pressure distribution. The resulting non-dimensional modified Reynolds equation in cylindrical coordinates, which governs the fluid film pressure evolution is given in Eq. (7), with the different coefficients summarized in the Appendix. The following assumptions are made for deriving the modified Reynolds equation:

1. The lubricant is a perfect gas operated in laminar conditions.
2. The fluid film is isothermal with a constant viscosity.
3. The pumping grooves are symmetrical, thus no axial mass flow is established within the fluid film.
4. The bearing edges are exposed to the same ambient conditions.

$$\partial_\varphi \left[\overline{P} \left(f_1 \partial_\varphi \overline{P} + f_2 \partial_{\bar{z}} \overline{P} \right) \right] + \partial_{\bar{z}} \left[\overline{P} \left(f_2 \partial_\varphi \overline{P} + f_3 \partial_{\bar{z}} \overline{P} \right) \right] + c_s \left[\sin\beta \partial_\varphi \left(\overline{P} f_4 \right) - \cos\beta \partial_{\bar{z}} \left(\overline{P} f_4 \right) \right] - \Lambda \partial_\varphi \left(\overline{P} f_5 \right) - \sigma \partial_{\bar{t}} \left(\overline{P} f_5 \right) = 0 \tag{7}$$

Lund's perturbation method is applied to compute the linearized bearing tilting impedance [14]. However, rather than perturbing the fluid film with a purely radial motion, a tilting perturbation by $\Delta\phi$ and $\Delta\theta$ is applied at a concentric bearing position around the x and y-axis as follows:

$$\overline{h} = 1 + \frac{\Delta\phi R}{h_r} \bar{z} \cos\varphi e^{i\bar{t}} + \frac{\Delta\theta R}{h_r} \bar{z} \sin\varphi e^{i\bar{t}} \tag{8}$$

The tilting motion clearance perturbation leads to a perturbation of the fluid film pressure as follows:

$$\overline{P} = \overline{P}_0 + \overline{P}_\phi e^{i\bar{t}} + \overline{P}_\theta e^{i\bar{t}} \tag{9}$$

Introducing Eq. (8) and (9) into Eq. (7) and collecting the zeroth and first order terms allows to obtain three linearized differential equations, one for the unperturbed pressure $\overline{P}_0$ and two for the perturbed pressure distribution resulting from the harmonic fluid film excitation in $\Delta\phi$ and $\Delta\theta$, $\overline{P}_\phi$ and $\overline{P}_\theta$, respectively. The bearing tilting impedances $Z_{ij} = K_{ij} + i\gamma \Omega_{Rot} C_{ij}$ are the obtained by integrating the perturbed pressure within the fluid film and projecting the resulting force around the x- and y-axes respectively:

$$Z_{\phi\phi} = -\int_{-L/D}^{L/D} \int_0^{2\pi} \overline{P}_\phi \bar{z} \cos\varphi d\varphi d\bar{z} \tag{10}$$

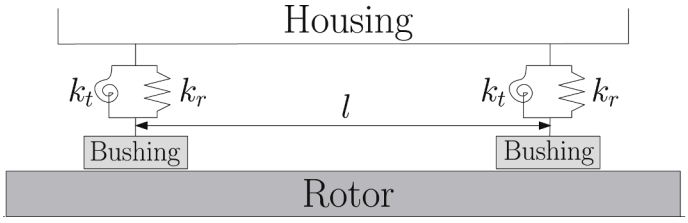

Fig. 2. Conceptual sketch of rotor flexibly supported by two HGJB bushings.

$$Z_{\phi\phi} = -\int_{-L/D}^{L/D}\int_{0}^{2\pi} \overline{P}_{\phi}\bar{z}\sin\varphi d\varphi d\bar{z} \tag{11}$$

Considering that the calculation of the impedances is performed in a concentric bearing configuration, the following simplification can be applied:

$$\begin{aligned} Z_{ii} &= Z_{jj} \\ Z_{ij} &= -Z_{ji} \end{aligned} \tag{12}$$

Fig. 3 represents the predicted synchronous tilting impedance of the HGJB supporting the test rotor using the model introduced in this section. The details of the bearing design are summarized in Table 1. The bearing impedance is clearly cross-coupled for both the stiffness and the damping matrices, which is a clear indication of a limited stability threshold in the bushing tilting motion.

2.2. Simplified method to evaluate bushing tilting Eigenfrequency

A simplified method to estimate the natural frequency of the bushing tilting mode is presented in Eq. (13), which assumes that the tilting stiffness of the flexible support is considerably higher than the stiffness of the gas film and therefore neglects the influence of the gas film tilting stiffness to predict the Eigenfrequency of the tilting mode.

$$\omega_{crit} = \sqrt{\frac{k_t}{J_{T_B}}} \tag{13}$$

2.3. Prototype description

The prototype and instrumentation used to experimentally investigate the flexible bearing bushing support is presented in Fig. 4. The rotor is supported on two HGJB bushings on the front and the back of the rotor, which are flexibly mounted in the housing by two identical flexible membrane supports as shown in Fig. 1.

Table 1 summarizes the rotor and bearing configuration of the prototype used to investigate the flexibly supported bearing bushings. Details about the design of the tunable flexible membrane support are given by Bättig and Schiffmann [2].

2.4. Measurement setup

Due to the impedance of the gas film, the orbital motion of the rotating shaft is transmitted to the flexibly supported bearing bushings. Any potential instability of the rotor-bearing-system can therefore be detected by measuring the motion of the bearing bushings. Furthermore, measurement of the bearing bushing motion allows to balance the rotor shaft in situ using the influence coefficient method [15].

The signature of an unstable gas bearing supported rotor due to self-excited whirl is the presence of sub-synchronous vibrations [12,16]. Hence, it is common practice to measure the rotor orbits on two planes and to analyze their frequency spectrum.

On the prototype used for this analysis, the motion of each bearing bushing is constantly monitored using two LionPrecision capacitance displacement probes and can be extended to include two Philtec D20 optical displacement probes to distinguish between the bushing radial and tilting motion. The motion of each bearing bushing is therefore captured by measuring its displacement in four different locations. The probe locations are shown in Fig. 5, where the motion in x- and y-direction is monitored using two

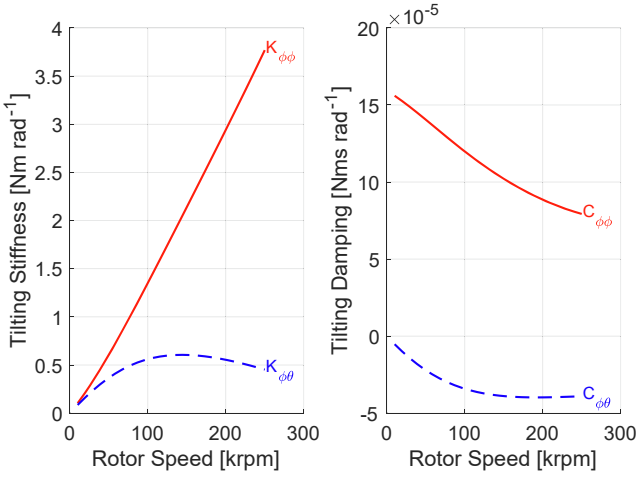

Fig. 3. HGJB synchronous tilting impedance as a function of the rotor speed.

Table 1
Rotor, bearing and bushing design parameters.

Bearing diameter D_{Brg}	10 mm
Bearing L_{Brg}/D_{Brg} ratio	1
Bearing groove width α	0.65
Bearing groove angle β	161
Bearing clearance h_r	9 μm
Bearing groove depth h_g	13 μm
Bearing groove length γ_{Brg}	1
Rotor mass m_R	0.0289 kg
Bushing mass m_B	4.102e-03 kg
Polar rotor inertia J_P	4.3258e-07 kg m^2
Transverse rotor inertia J_{T_R}	1.8112e-05 kg m^2
Transverse bushing inertia J_{T_B}	1.219e-07 kg m^2
Bearing distance l	58.5 mm
Nominal rotor speed N_{Rot}	250 krpm
Radial bushing support stiffness k_r	0.9e6 N m^{-1}
Tilting bushing support stiffness k_t	4.3 N m rad^{-1}

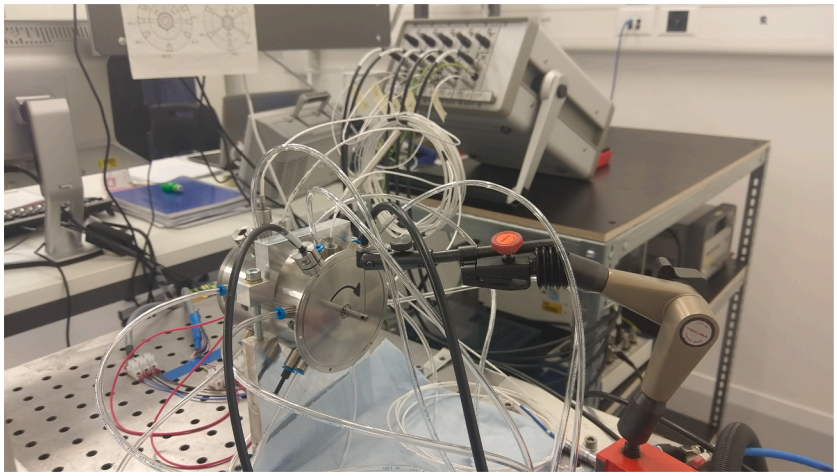

Fig. 4. Prototype with implemented flexible membrane bushing support and instrumentation.

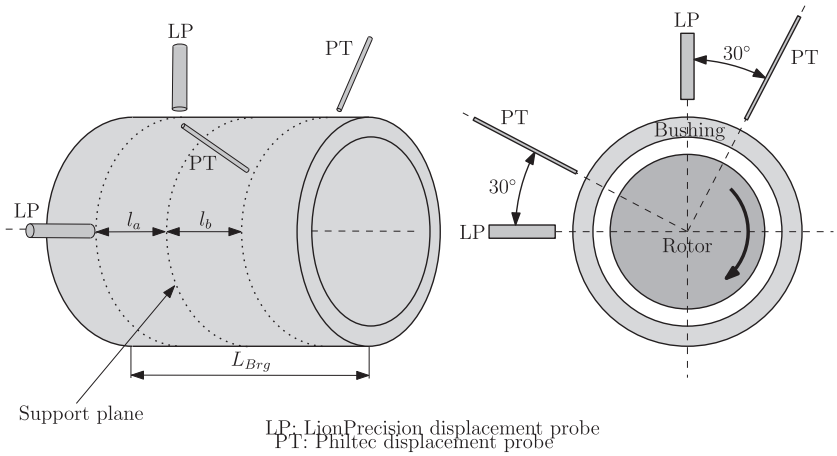

Fig. 5. Location of LionPrecision and Philtec displacement probes on bearing bushing.

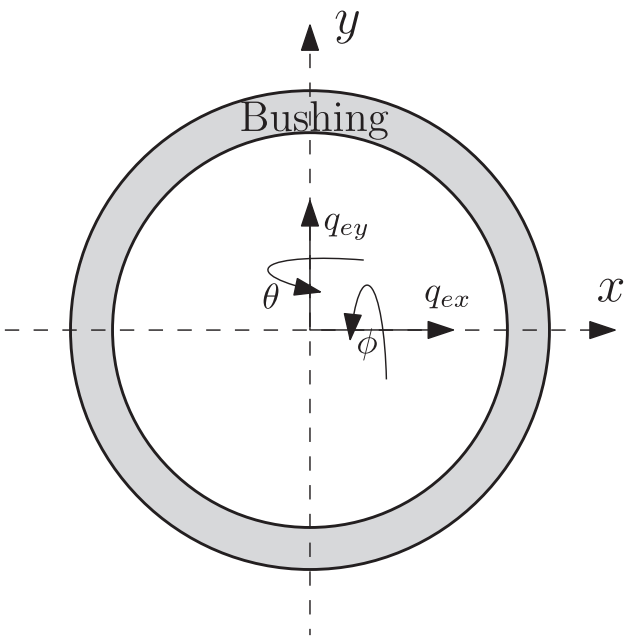

Fig. 6. Transformation of measurement data to a cylindrical and a tilting movement in the center of the bearing bushing.

LionPrecision capacitance displacement probes on one side of the flexible membrane support and two Philtec D20 optical displacement probes on the other side of the flexible membrane support, shifted by 30 deg relative to the x- and y-direction due to space limitations. l_a represents the distance of the LionPrecision measurement plane to the center plane of the bearing bushing, whereas l_b is the distance of the Philtec measurement plane to the bushing center plane. The distances l_a and l_b measure 3.25 mm and 2.75 mm respectively. Table 2 lists the relevant measurement equipment used to investigate the bushing tilting motion.

2.5. Measurement analysis procedure

The motion of a rigid body in the x- and y-plane can be described completely if two translational and two rotational degrees of freedom of any point of the rigid body are known. By defining a master node, the motion of any slave node can therefore be calculated using a rigid-body-transformation matrix $\mathbf{T_{ms}}$ [17]. The transformation matrix $\mathbf{T_{ms}}$ transforms the degrees of freedom of the master node $\overrightarrow{\mathbf{q_m}}$ into the degrees of freedom of the slave nodes $\overrightarrow{\mathbf{q_s}}$, as presented in Eq. (14).

$$\overrightarrow{\mathbf{q_s}} = \mathbf{T_{ms}} \cdot \overrightarrow{\mathbf{q_m}} \tag{14}$$

By defining the center of the bearing bushing as the master node, with four degrees of freedom q_{ex}, q_{ey}, ϕ and θ, the displacement in x- and y-direction at each measurement location can be predicted. Reversing this procedure, as shown in Eq. (15), allows to reduce the measurement data from the four measurement locations presented in Fig. 5 into translational and tilting motion components of the bearing bushing.

$$\overrightarrow{\mathbf{q_m}} = \mathbf{T_{ms}^{-1}} \cdot \overrightarrow{\mathbf{q_s}} \tag{15}$$

The translational degrees of freedom of the bearing bushing center q_{ex} and q_{ey}, as well as to two tilting degrees of freedom ϕ and θ around the x- and y-axis respectively, are shown in Fig. 6. During post-processing, the complete set of measurement data in the time-domain is transformed according to Eq. (15), followed by a spectral analysis performed on both the translational and the tilting degrees of freedom of the bearing bushing center. This procedure allows to determine whether a potential instability has its origin in a translational or in a tilting motion mode.

Table 2
List of instrumentation.

Device	Model
Capacitive displacement probes	LionPrecision C3S
Optical displacement probes	Philtec D20
Signal amplifier	Lion Precision CPL290
DAQ system	NI PXIe-1078/6356

3. Results and discussion

3.1. Identification of an unstable bushing tilting mode

The synchronous and sub-synchronous motion amplitudes recorded on the flexibly supported bearing bushing during a speed ramp up to 116 krpm are presented in Fig. 7. The radial stiffness k_r of the flexible support is 0.9e + 06 Nm^{-1}, while the tilting stiffness k_t is 4.3 Nm rad^{-1}. The presented measurement results are captured with the two LionPrecision displacement probes located on the back measurement plane of the bearing bushing according to Fig. 5.

The evolution of the sub-synchronous motion amplitude presents a steady increase until 110 krpm, after which the rise progresses much steeper until 116 krpm, at which point the sub-synchronous vibration amplitude exceeds the synchronous amplitude, suggesting the onset of an instability in the bearing bushing or rotor motion. The rotor speed of 116 krpm was not exceeded in order to avoid a failure of the prototype. After the decomposition of the measurement signals into a translational and a tilting motion, a frequency spectrum analysis is performed on each bushing degree of freedom separately and plotted in Fig. 8.

The translational spectrum shows a steadily increasing amplitude suggesting that the translational Eigenfrequency has not been crossed yet. The absence of a clear sub-synchronous component also suggests a fully stable translational motion. The tilting spectrum, however, shows a peak amplitude around 1 kHz, thus suggesting a tilting Eigenfrequency, which corroborates with the orbit measurement evolution in Fig. 7. Further, the spectrum clearly shows a steeply rising sub-synchronous peak, suggesting an unstable tilting motion of the flexibly supported bearing bushing. The results clearly suggest that the origin of the observed instability is caused by an instability of the bearing bushing in a tilting motion mode.

This analysis also corroborates with the visualization of the motion of the bushings based on the experimental data and plotted in Fig. 9 for various discrete rotor speeds corresponding to the ones highlighted in Fig. 7 through the numbered vertical dotted lines. The orbit plots clearly indicate clean circular orbits suggesting stable operation up to a rotor speed of approximately 90 krpm (line 5) after which the tilting motion becomes increasingly noisy showing clear patterns of a superposed sub-synchronous component suggesting the onset of a bushing tilting instability.

These measurements are clearly offering experimental proof that a flexibly supported bushing of a gas lubricated bearing can experience unstable motion not only in translational but also in tilting motion. It is therefore suggested that the design process of gas bearings on flexible supports needs to account also for this particular motion to ensure stable operation.

3.2. Effect of support tilting stiffness on onset speed of bushing instability

The measured synchronous motion amplitudes measured on the bearing bushing for four different support tilting stiffness levels k_t all with the same radial stiffness k_r are presented in Fig. 10 as a function of rotor speed. The plot clearly highlights that an increase in tilting stiffness also increases the rotor speed at which highest motion amplitude occurs.

Fig. 11 presents the predicted whirl speed map for the bushing tilting motion and the corresponding evolution of the logarithmic decrement as a function of the rotor speed for the four investigated tilting stiffness levels based on the reduced order model introduced

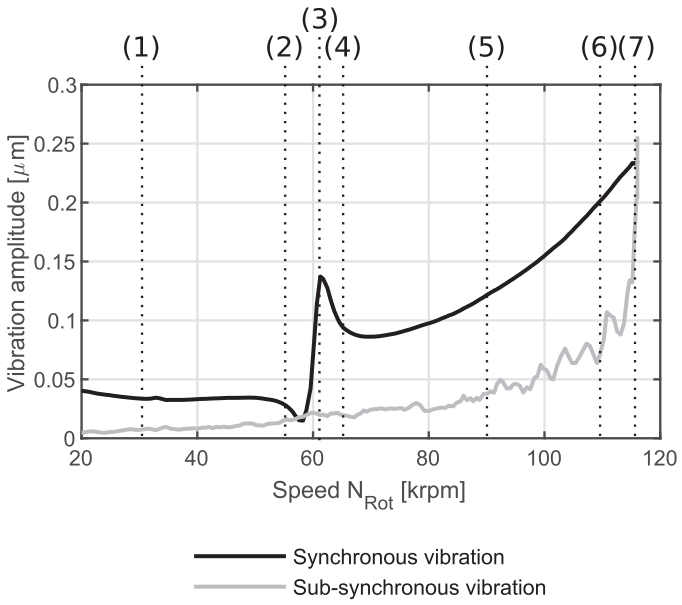

Fig. 7. Recorded synchronous and sub-synchronous motion amplitudes of flexibly supported bearing bushing ($k_r = 0.9e + 06$ N m^{-1}, $k_t = 4.3$ N m rad^{-1}) as a function of rotor speed.

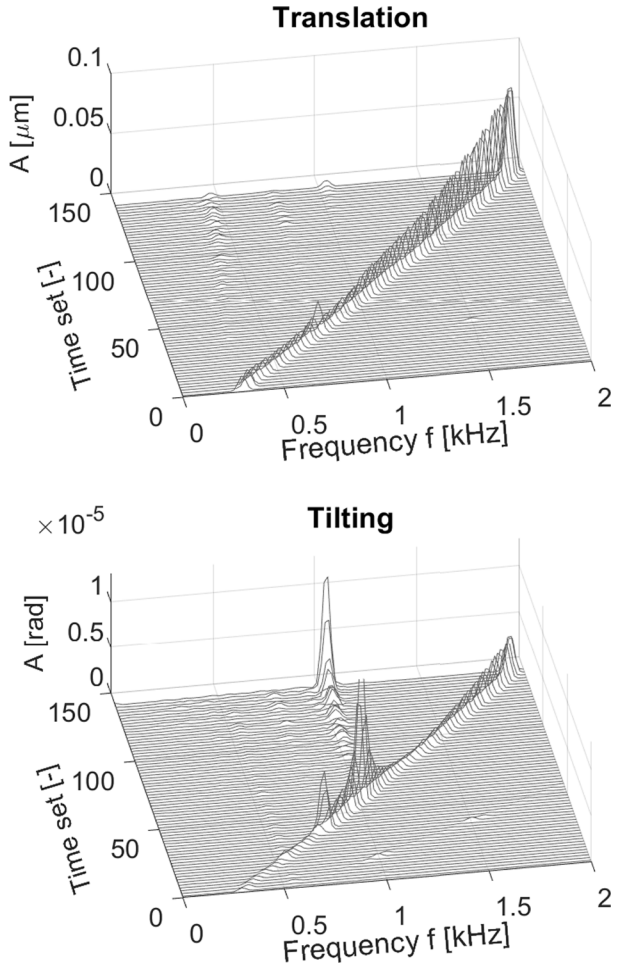

Fig. 8. Measured frequency spectrum of bushing translational and bushing tilting motion for k_r = 0.9e + 06 N m^{-1} and k_t = 4.3 N m rad^{-1}.

above. For illustrational purpose, only the critical speeds and the logarithmic decrements of the forward modes are plotted, since the backward modes are well damped and therefore do not present any concern for instability. The occurrence of negative logarithmic decrements predicted by the dynamic model, and hence unstable motion, clearly suggests that the unstable behavior of the bushing tilting motion can be attributed to the cross-coupled characteristics of the tilting impedance of the gas bearing. Further, the predicted results suggest an increase in critical speed with increasing tilting stiffness of the flexible support, which corroborates with the experimental results presented in Fig. 10. The rotordynamic model predicts the critical speed of the bushing tilting modes (intersection of Eigenfrequencies with parity line) to be at 60 krpm, 123 krpm, 140 krpm and 251 krpm.

For the sake of comparison, the measured Eigenfrequencies and the predicted ones obtained from the bushing tilting model and the simplified model (Eq. (13)) are summarized in Table 3. The obtained prediction results using the bushing tilting model match the measured critical speeds very well with the largest deviation of 5.7% occurring for the flexible support with a tilting stiffness k_t of 28.3 Nm rad^{-1}, whereas a deviation of 7.8% is obtained when using the simplified prediction model at the same tilting stiffness. Notice that the simplified model is obtained under the assumption that the tilting stiffness contribution from the gas bearing is negligible compared to the one from the bushing support. The relatively small difference between the two models in predicting the bushing tilting Eigenfrequency seems to support this assumption, which corroborates with the ratio between the flexible support stiffness and the tilting stiffness of the bearing (Fig. 3) ranging between 0.05 and 0.25 for the 4 tested support tilting stiffness.

The evolution of the calculated logarithmic decrement Γ_{Bush} with rotational speed, presented in Fig. 11(b), suggests the speed of instability onset (SIO) of the bushing tilting motion to increase with increasing flexible support tilting stiffness. The predicted tilting speed of instability onset (SIO) for a tilting stiffness k_t = 4.3 N m rad^{-1} at 119 krpm corroborates very well the experimentally determined SIO of 116 krpm. The predicted SIO for a tilting stiffness k_t of 21.8 N m rad^{-1} is at 202 krpm. Due to the fatal consequences of a crash at such a high rotational speed, the SIO has not been experimentally verified, however, a speed of 185 krpm was obtained with this support tilting stiffness without any sign of instability. Supporting the bearing bushings with a tilting stiffness of k_t = 28.3 N m rad^{-1} is suggested to allow stable operation up to 230 krpm according to the prediction results shown in Fig. 11(b). Again, no experimental verification of the SIO was performed due to a high risk of crashing the prototype. However, a safe speed of 200 krpm was

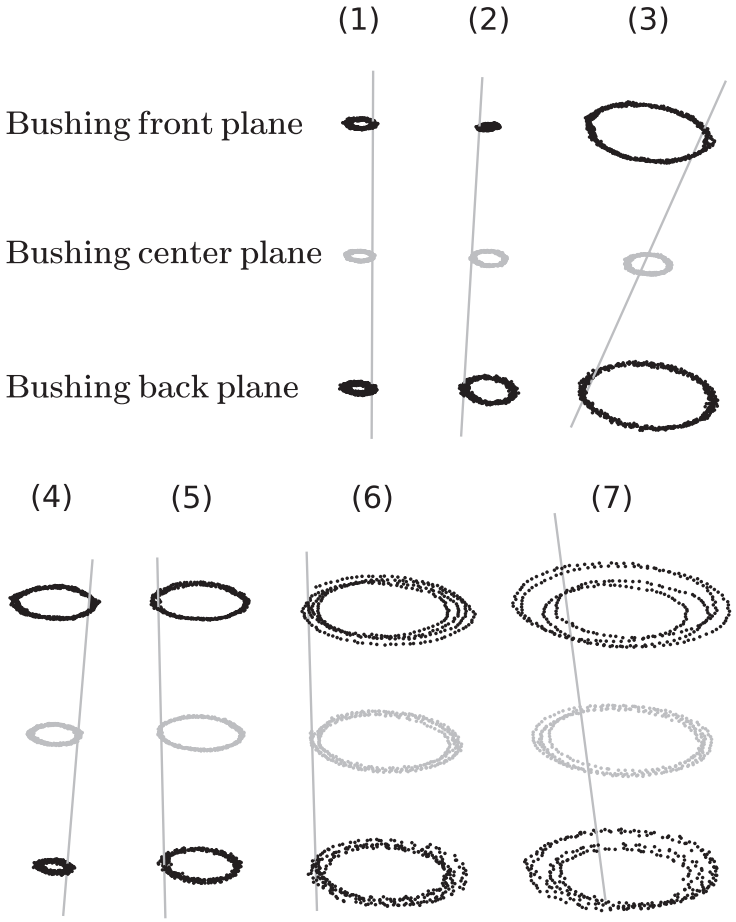

Fig. 9. Bushing motion at selected speeds indicated in Fig. 7 on flexible support ($k_r = 0.9\text{e}+06$ N m^{-1}, $k_t = 4.3$ N m rad^{-1}).

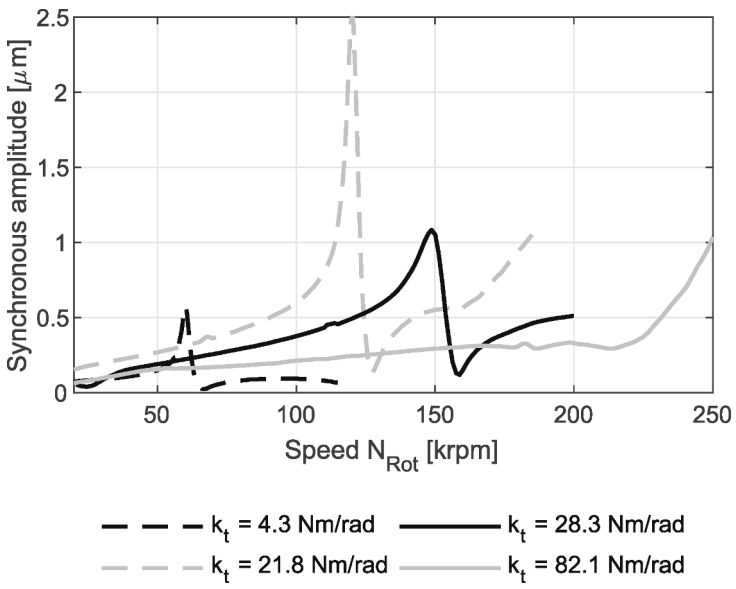

Fig. 10. Comparison of synchronous bearing bushing motion amplitudes for different tilting stiffnesses k_t with $k_r = 0.9\text{e}+06$ N m^{-1} as a function of rotor speed.

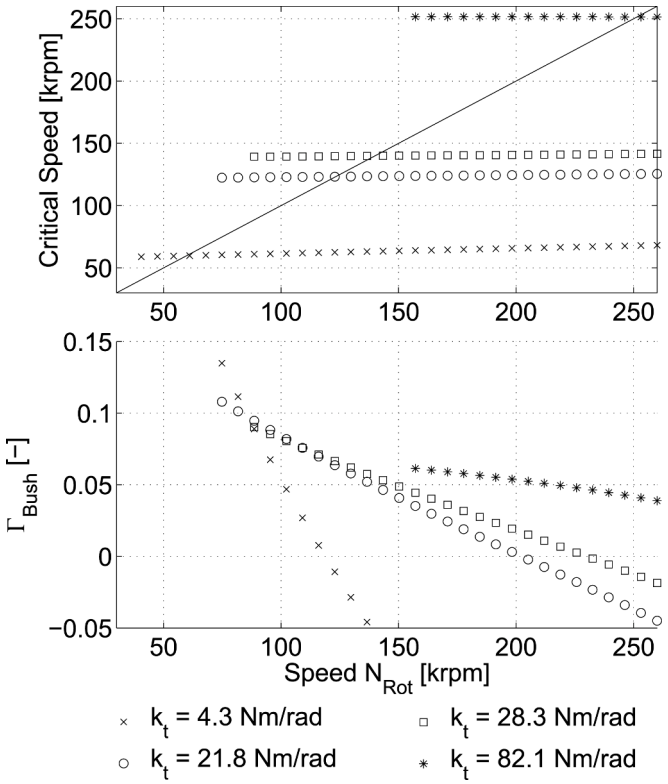

Fig. 11. Influence of membrane tilting stiffness. (a) Predicted critical speed of bearing bushing tilting mode; (b) Logarithmic decrement Γ_{Bush}.

Table 3
Comparison of measured bushing tilting Eigenfrequencies with model predictions.

Tilting stiffness k_t N m rad^{-1}	**Exp.** kHz	**Model** kHz	**Simplified Model** kHz
4.3	0.99	1	0.95
21.8	2	2.05	2
28.3	2.47	2.33	2.28
82.1	4.2	4.18	4.13

reached and no sub-synchronous vibrations detected.

According to the model prediction, a minimum tilting stiffness of $k_t = 40$ N m rad^{-1} is required to allow stable operation ($\Gamma_{Bush} \geqslant 0$) over the whole speed range up to 250 krpm. A flexible support with a tilting stiffness of $k_t = 82.1$ N m rad^{-1} was designed, therefore offering a high margin against bush tilting instability in the nominal speed range up to 250 krpm.

Fig. 12 presents the frequency spectrum of the measured bushing motion during a speed ramp from 0 to 250 krpm for the front and back bearing bushings supported on the flexible support offering a tilting stiffness k_t of 82.1 N m rad^{-1}. The absence of any sub-synchronous vibrations (both translational and tilting) suggests stable operation of the prototype up to 250 krpm, which is in agreement with the prediction of the rotordynamic model. The good agreement between the predicted and the measured Eigenfrequency further emphasizes the accuracy of the reduced order model.

3.3. *Effect of bushing transverse moment of inertia on bushing tilting stability*

Fig. 13 presents the motion amplitude of the bearing bushing supported on a flexible support with $k_r = 0.9\text{e}+06$ N m^{-1} and $k_t = 4.3$ N m rad^{-1} and compares it to the motion amplitude of the same bushing on an identical flexible support but with a total transverse moment of inertia of the bushing J_{Ttot} increased by 37% by means of an additional metal ring fitted on the bushing. The prominent peak at 60 krpm for the low inertia bearing bushing, has previously been identified as the critical speed of the bearing bushing tilting mode. As suggested by the measurement data, the critical speed of this tilting mode decreases from 60 krpm to 51 krpm due to the increased transverse mass moment of inertia caused by the additional ring.

Fig. 14 presents the frequency spectra obtained by FFT for the tilt angle θ of the flexibly supported bearing bushing with and without additional ring. In both experiments, the speed is increased until a sub-synchronous motion component is detected in the

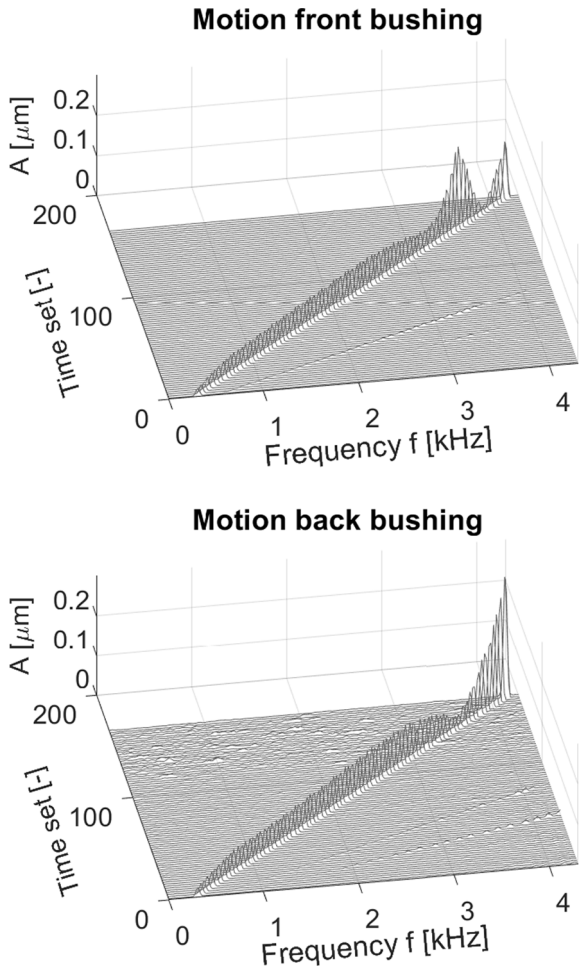

Fig. 12. Measured frequency spectrum of the bushing motion (tilting and tranlalation) for a flexible support with a tilting stiffness k_t of 82.1 N m rad^{-1}: (a) Front bearing bushing; (b) Back bearing bushing.

frequency spectrum. Both spectra show an increase of the synchronous frequency with speed, which is due to the residual rotor imbalance. The spectra also show the presence of sub-synchronous vibration in the tilting motion of the bushing. However, the speed of instability onset is decreased for the bearing bushing featuring an increased transverse moment of inertia J_{Ttot}. The spectrum of the test with the lower J_{Ttot} bushing presents the appearance of sub-synchronous bushing tilting vibrations at a synchronous vibration frequency of 1930 Hz, corresponding to a speed of 116 krpm, whereas the sub-synchronous vibrations for the bushing with increased inertia (Fig. 14(b)) start appearing at 1783 Hz, which represents a rotational speed of 107 krpm. The sub-synchronous vibrations occur at a frequency of 1000 Hz and 850 Hz for the low inertia and high inertia bearing bushing respectively, corresponding to the critical speed of 60 krpm and 51 krpm of the bush tilting mode, as presented in Fig. 13.

The critical bushing tilting whirl speed ratio γ_{crit}, defined as the ratio of sub-synchronous to synchronous vibration frequency at the onset of instability, is 0.52 and 0.48 for the low inertia and high inertia bearing bushing respectively, representing a typical half-frequency whirl.

The comparison of the experimental data obtained with the same support characteristics but with different transverse bushing inertia clearly suggests a strong impact of the inertia on both the onset speed of instability and the critical speeds related to the tilting motion of the flexibly supported bushing.

Fig. 15(a) presents the predicted critical speed of the forward and backward bearing bushing tilting modes for the high and low inertia bushings supported on the flexible support with a tilting stiffness k_t of 4.3 N m rad^{-1}, while Fig. 15(b) shows the evolution of the corresponding logarithmic decrement Γ_{Bush}. As suggested by the predicted whirl speed map (Fig. 15(a)), the critical speed of the bushing tilting mode decreases from 60 krpm to 51 krpm for a 37% increase of the transverse bushing inertia, matching exactly the observed critical speeds presented in Fig. 13. The predicted speed of instability onset of the bushing tilting mode ($\Gamma_{Bush} < 0$) for a support stiffness $k_t = 4.3$ N m rad^{-1} is at 119 krpm for the low inertia bushing, which agrees very well with the observed start of sub-synchronous vibrations at 116 krpm, visible in the frequency spectrum in Fig. 14. The numerical model predicts the speed of instability onset for the bushing tilting motion to drop from 119 krpm to 100 krpm for the increased transverse bushing inertia. The measurement

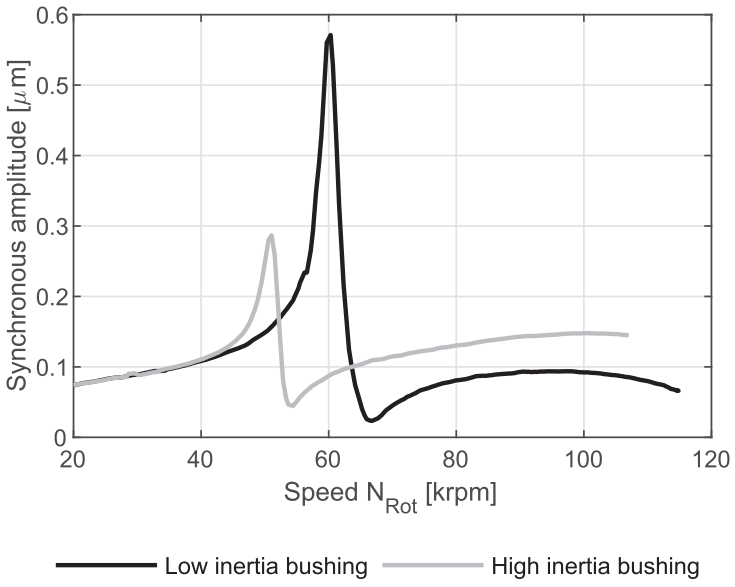

Fig. 13. Comparison of back bearing bushing motion amplitudes for a high and a low transverse inertia bushing.

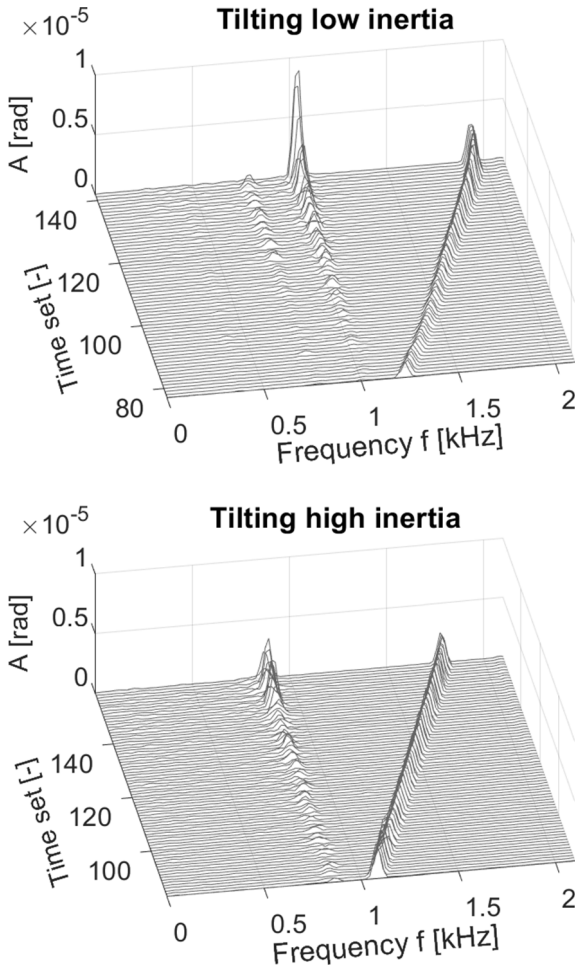

Fig. 14. FFT spectrum of back bushing tilt angle θ: (a) Original; (b) Increased bushing transverse moment of inertia (J_{Ttot} + 37%).

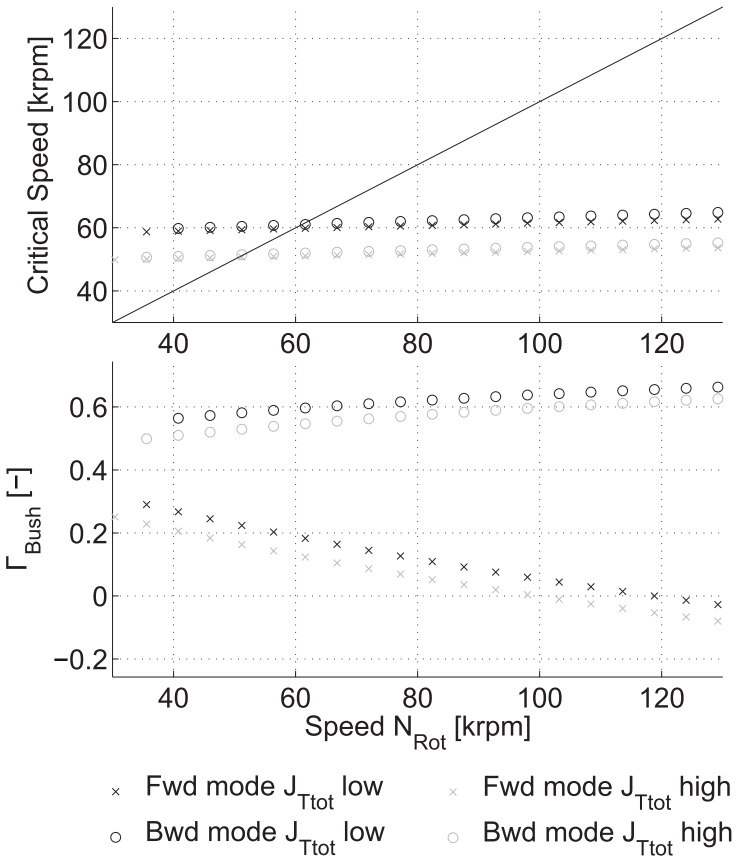

Fig. 15. Influence of the bushing transverse moment of inertia. (a) Predicted critical speed of bearing bushing tilting mode; (b) Logarithmic decrement Γ_{Bush}.

results suggest the onset speed of instability to be at 107 krpm for the high inertia bushing, 7% higher than the prediction obtained from the rotordynamic model. As suggested by the evolution of the logarithmic decrement Γ_{Bush}, the backward tilting motion remains stable over the whole investigated speed range.

3.4. Effect of damping on bushing tilting stability

The addition of external damping to the motion of the bearing bushing is suggested to increase the speed of instability onset [6]. The introduction of damping and its effect on the bushing tilting instability was experimentally tested by adding a friction disk to the flexible bearing bushing support. The friction disk consists of an axially pre-loaded disk that creates friction during the tilting motion of the bearing bushing and hence results in Coulomb damping [2]. Fig. 16 presents the frequency spectra of the measured bearing bushing tilting motion with and without damping supported on the same flexible support ($k_t = 4.3$ Nmrad^{-1}). The measured spectra clearly suggest that the introduction of damping significantly increases the onset speed of bushing tilting instability. According to the presented measurement results, the additional external damping provided by the friction disk allows to increase the onset of instability of the bush tilting mode from 116 krpm to 160 krpm, which represents an extension of the stable speed range by 38%.

3.5. Simplified design guideline

The 2 degrees of freedom reduced-order model presented in this paper allows to predict whirl speed and stability maps of flexibly supported herringbone grooved journal bearing bushings in excellent agreement with experimental data. Good agreement with measurements is also obtained with the simplified model to determine the Eigenfrequency of the bushing tilting mode (Eq. (13)). Since the whirl speed ratio of instability onset γ_{crit} is generally $\leqslant 0.5$, it is suggested that the following criteria has to be fulfilled to avoid the bushing tilting mode to become unstable in the nominal speed range:

$$\omega_{crit} > 0.5 \cdot \omega_{rot} \tag{16}$$

where the critical frequency ω_{crit} of the bushing tilting mode is evaluated according to Eq. (13). This approach is neglecting the stiffness of the gas film, which therefore results in a conservative, yet simple to apply design guideline.

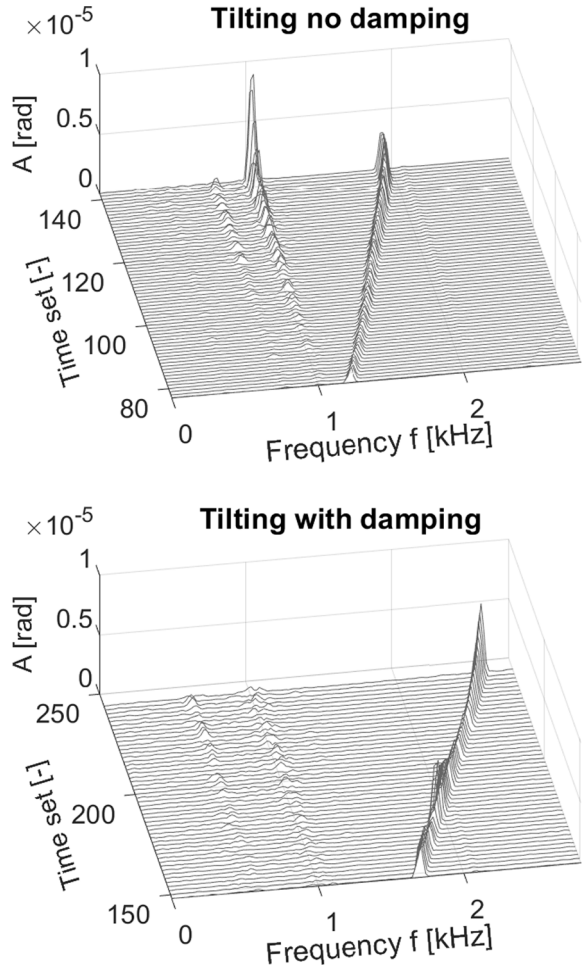

Fig. 16. Frequency spectrum of bearing bushing tilting on a flexible support without damping (top) and on a flexible support with damping (bottom).

4. Conclusions

An experimental method based on proximity probe measurements to distinguish between translational and tilting motion of flexibly supported herringbone grooved journal bearing bushings has been introduced and used to identify the occurrence of an unstable tilting motion of the flexibly supported bearing bushing. As expected for gas bearing supported rotor instabilities, the tilting instability of the bushing manifested in the appearance of a typical sub-synchronous signature in the signal frequency spectrum.

The introduction of a two degrees of freedom reduced-order model of the tilting motion of the gas bearing bushing allowed to investigate the effect of the bushing transverse moment of inertia, the tilting stiffness of the flexible bushing support and the introduction of damping on the onset speed of bushing tilting instability. The reduced order model includes the dynamic specifications of the flexible bushing support as well as the gas bearing impedance. The effect of bushing inertia, tilting stiffness and damping on the onset speed of bushing tilting instability were also experimentally investigated, which allowed a validation of the reduced-order model. The comparison between the dynamic model and experimental data suggests modeling errors $< 7\%$ with regards to both the bushing Eigenfrequency and the rotor speed at the onset of instability.

Both the dynamic model as well as experimental data suggest that an increase in the flexible bushing tilting stiffness increases the speed of tilting instability onset, while an increase in the bushing transverse moment of inertia results lowers the onset speed of instability. Further, the introduction of damping through the flexible support allows to significantly increase the onset speed of the tilting instability.

The experimental data in conjunction with a simplified model, that enables to estimate the natural frequency of the bush tilting mode, based on the bushing transverse inertia and the flexible support tilting stiffness enabled the definition of a design guideline, which allows designers to avoid a bushing tilting mode to become unstable within the operating speed range of a prototype.

CRediT authorship contribution statement

Philipp Bättig: Conceptualization, Methodology, Software, Investigation, Visualization, Data curation, Writing - original draft. **Jürg Schiffmann:** Supervision, Funding acquisition, Software, Writing - review & editing.

Declaration of Competing Interest

The authors declare that they have no known competing financial interests or personal relationships that could have appeared to influence the work reported in this paper.

Acknowledgement

This work was supported by the Swiss National Science Foundation under Grant PYAPP2_154278/1.

Appendix A

The Narrow Groove Theory coefficients for the modified Reynolds equation (Eqn. 7) are summarized as follows:

$$
\begin{aligned}
&\overline{h}_r = \frac{h_r}{h_0}\\
&\overline{h}_g = \frac{h_g}{h_0}\\
&H = \frac{h_g}{h_0}\\
&g_1 = \overline{h}_g^3\overline{h}_r^3\\
&g_2 = \left(\overline{h}_g^3 - \overline{h}_r^3\right)^2\alpha(1-\alpha)\\
&(1-\alpha)\overline{h}_g^3 + \alpha\overline{h}_r^3\\
&c_s = -\frac{6\mu\Omega_{Rot}R^2}{p_a h_0^2}\alpha(1-\alpha)(H-1)\sin\beta\\
&f_1 = \frac{g_1 + g_2\sin\beta}{g_3}\\
&f_2 = \frac{g_2\sin\beta\cos\beta}{g_3}\\
&f_3 = \frac{g_1 + g_2\cos\beta}{g_3}\\
&f_4 = \frac{\overline{h}_g^3 - \overline{h}_r^3}{g_3}\\
&f_5 = \alpha\overline{h}_g + (1-\alpha)\overline{h}_r\\
&\Lambda = \frac{6\mu\Omega_{Rot}}{p_a}\left(\frac{R}{h_r}\right)^2\\
&\sigma = \frac{12\mu\Omega_{Rot}\gamma}{p_a}\left(\frac{R}{h_r}\right)^2
\end{aligned}
\tag{1}
$$

References

[1] E. Guenat, J. Schiffmann, Multi-Objective Optimization of Grooved Gas Journal Bearings for Robustness in Manufacturing Tolerances, Tribology Transactions 62 (6) (2019) 1041–1050, ISSN 1040-2004, 1547-397X, doi: 10.1080/10402004.2019.1642547.
[2] P. Bättig, J. Schiffmann, Flexible Support for Gas Lubricated Bearing Bushings, Tribol. Trans. (2020) 1–27, https://doi.org/10.1080/10402004.2020.1717702.

[3] G. Belforte, F. Colombo, T. Raparelli, V. Viktorov, High-speed rotor with air bearings mounted on flexible supports: test bench and experimental results, J. Tribol. 130 (2) (2008), 021103, https://doi.org/10.1115/1.2908905.
[4] T. Waumans, J. Peirs, F. Al-Bender, D. Reynaerts, Aerodynamic Journal Bearing with a Flexible, Damped Support Operating at 7.2 Million DN, Journal of Micromechanics and Microengineering 21 (10) (2011) 104014, doi: 0.1088/0960-1317/21/10/104014.
[5] T. Waumans, J. Peirs, F. Al-Bender, D. Reynaerts, DESIGN, OPTIMISATION AND TESTING OF A HIGH-SPEED AERODYNAMIC JOURNAL BEARING WITH A FLEXIBLE, DAMPED SUPPORT, in: Technical Digest PowerMEMS, Washington DC, USA, 83–86, 2009.
[6] N. Miyanaga, J. Tomioka, Effect of support stiffness and damping on stability characteristics of herringbone-grooved aerodynamic journal bearings mounted on viscoelastic supports, Tribol. Int. 100 (2016) 195–203, https://doi.org/10.1016/j.triboint.2016.01.019.
[7] J. Tomioka, N. Miyanaga, Measurement of Dynamic Properties of O-rings and Stability Threshold of Flexibly Supported Herringbone Grooved Aerodynamic Journal Bearings, Tribology Online 3 (7) (2008) 366–369, https://doi.org/10.2474/trol.3.366.
[8] J. Tomioka, N. Miyanaga, Stability Threshold of Herringbone Grooved Aerodynamic Journal Bearings with External Stiffness and Damping Elements, J. Adv. Mech. Design, Syst., Manuf. 7 (6) (2013) 876–887, https://doi.org/10.1299/jamdsm.7.876.
[9] K. Somaya, M. Miyatake, K. Okubo, S. Yoshimoto, Threshold Speed of Instability of a Herringbone-Grooved Rigid Rotor with a Bearing Bush Flexibly Supported by Straight Spring Wires, in: Proceedings of ASME Turbo Expo 2015: Turbine Technical Conference and Exposition GT2015, vol. 7A, Montreal, Canada, V07AT31A015, 2015.
[10] S. Yoshimoto, M. Miyatake, K. Nagata, Instability of herringbone grooved aerodynamic floating bush bearings flexibly supported by foils with hemispherical bumps, in: Proceedings of ASME/STLE International Joint tribology Conference, San Diego, California, USA, 261–263, 2007.
[11] C.H. Pan, Spectral Analysis of Gas bearing systems for Stability Studies, Tech. Rep. 64TR58, MTI, 1964.
[12] J.H. Vohr, C.Y. Chow, Characteristics of Herringbone-Grooved, Gas-Lubricated Journal Bearings, J. Basic Eng. 87 (1965) 568–578.
[13] E. Guenat, J. Schiffmann, Dynamic force coefficients identification on air-lubricated herringbone grooved journal bearing, Mechanical Systems and Signal Processing 136 (2020) 106498, ISSN 0888-3270, doi: 10.1016/j.ymssp.2019.106498.
[14] J.W. Lund, Calculation of Stiffness and Damping Properties of Gas Bearings, J. Lubr. Technol. 90 (4) (1968) 783–803.
[15] M.S. Darlow, Influence Coefficient Balancing, in: Balancing of High-Speed Machinery, Mechanical Engineering Series, chap. 6, Springer New-York, NY, USA, 81–106, 1989.
[16] D.D. Fuller, A Review of the State-of-the-Art for the Design of Self-Acting Gas-Lubricated Bearings, J. Lubr. Technol. 91 (1969) 1–16.
[17] O. Bottema, B. Roth, Theoretical Kinematics, Dover Books on Physics, Dover Publications, NY, USA, 2012.